12-2012

Projected changes of extreme weather events in the eastern United States based on a high resolution climate modeling system

Y Gao

J S. Fu
University of Tennessee - Knoxville

J B. Drake

Y Liu

J-F Lamarque

Projected changes of extreme weather events in the eastern United States based on a high resolution climate modeling system

Projected changes of extreme weather events in the eastern United States based on a high resolution climate modeling system

Y Gao[1]**, J S Fu**[1]**, J B Drake**[1]**, Y Liu**[2]** and J-F Lamarque**[3]

[1] Department of Civil and Environmental Engineering, University of Tennessee, Knoxville, TN, USA
[2] Rollins School of Public Health, Emory University, Atlanta, GA, USA
[3] Atmospheric Chemistry and Climate and Global Dynamics Divisions, National Center for Atmospheric Research, Boulder, CO, USA

E-mail: jsfu@utk.edu

Abstract

This study is the first evaluation of dynamical downscaling using the Weather Research and Forecasting (WRF) Model on a 4 km × 4 km high resolution scale in the eastern US driven by the new Community Earth System Model version 1.0 (CESM v1.0). First we examined the global and regional climate model results, and corrected an inconsistency in skin temperature during the downscaling process by modifying the land/sea mask. In comparison with observations, WRF shows statistically significant improvement over CESM in reproducing extreme weather events, with improvement for heat wave frequency estimation as high as 98%. The fossil fuel intensive scenario Representative Concentration Pathway (RCP) 8.5 was used to study a possible future mid-century climate extreme in 2057–9. Both the heat waves and the extreme precipitation in 2057–9 are more severe than the present climate in the Eastern US. The Northeastern US shows large increases in both heat wave intensity (3.05 °C higher) and annual extreme precipitation (107.3 mm more per year).

1. Introduction

Global climate models (GCMs) are designed to simulate large-scale global climate at a spatial resolution of several hundred kilometers [1]. However, finer spatial resolution has become increasingly important when studying the impact of climate change at the local level [2]. There are two primary

methods for studying climate change in more spatial detail: statistical downscaling and dynamical downscaling. Statistical downscaling establishes the empirical relationships between large-scale climate and local climate based upon statistical methods [3]. It demands less computational power and requires less effort to implement, but it is limited by assuming stationary relationship between present observations and the present model climate in a changed future climate [4]. Dynamical downscaling uses GCMs output to provide the initial and boundary conditions for the regional climate models (RCMs) projecting globally consistent high resolution local climate conditions [2]. It is computationally demanding

and requires considerable implementation effort, but a major advantage is the dependence on physical process rather than statistical correlations and there is no assumption of stationarity [3]. Thus, in order to capture extreme conditions and provide more regional detail, the dynamical downscale technique is used in this study.

Dynamical downscaling has been studied since the early 1990s [5–9]—using RCMs with spatial resolutions of 50–60 km. More recently, finer spatial resolution has been applied. Bell *et al* [10] conducted dynamical downscaling on a 40 km × 40 km resolution, and found 75% of RCMs perform similarly or more favorably than GCMs over 16 stations in California region. Salathe *et al* [11] evaluated daily maximum, minimum temperature and precipitation over 55 stations in the Northwestern US at 15 km resolution, and found a cold bias in downscaled RCM results, which is likely inherited from the GCM. Other high resolution downscaling studies were also conducted for California [2, 12, 13]. As these studies have a major focus in the western US, the high resolution dynamical downscaling was previously ignored in the eastern US. Since the small domain size in previous studies limits the number of observational data (only 16 in Bell *et al* [10] and 55 in Salathe *et al* [11]), it would be more meaningful and representative to evaluate a larger domain with more observational sites (more than 1000), thus the design of a larger eastern US domain in this study. In addition, most previous downscaling studies use National Center for Atmospheric Research (NCAR) GCM Parallel Climate Model (PCM) or Community Climate System Model version 3 (CCSM3). The PCM has been superseded by the CESM, which includes an updated atmosphere component, the Community Atmosphere Component version 4 (CAM4) [14]. Compared to CAM3 (in CCSM3) and PCM, CAM4 contains significant improvement on El Niño–Southern Oscillation (ENSO) by the inclusion of sub-grid scale convective momentum transport and a dilution approximation for the calculation of convective available potential energy (CAPE) in the deep convection [15]. To provide downscaling analysis with the new GCM model is the purpose of this study. At the end, the discussions of the newest Coupled Model Intercomparison Project Phase 5 (CMIP5) [16, 17] 'representative concentration pathways[4] (RCPs [18]) scenarios in this study could potentially contribute to the upcoming Fifth Assessment Report (AR5) of the United Nations Intergovernmental Panel on Climate Change (IPCC). Thus, the eastern US domain is targeted in this study with a high resolution (4 km × 4 km) to provide an understanding of the dynamics of climate change on a highly resolved regional basis.

A higher resolution is necessary for climate studies of extreme weather events [2]. Extreme weather events have already significantly influenced North America. According to Lott and Ross [19] nearly every year since 1980, extreme weather events have caused more than 1 billion dollars in damage in the US. Prior to 2005, four or fewer events occurred yearly; while 5 events were experienced in 2005, an extreme peak was reached with 14 events occurring in 2011.[5] In 2005

the annual loss due to extreme weather events totaled 100 billion dollars, mainly due to Hurricane Katrina. A more commonly occurring extreme event, heat waves, can inflict substantial harm on sensitive populations including the elderly and people with pre-existing health conditions. For instance, several hundred people died in 1995 during the Chicago heat wave and more than 30 000 deaths were attributed to the 2003 European heat wave [20, 21]. In 2010, about 55 000 premature deaths were attributed to the Russian heat wave ('2010 Disasters in Numbers' CRED[6]). In addition, more intense heat waves [22, 23] and precipitation [24] are likely to occur in a warmer climate. Thus, two kinds of extreme events, heat waves and extreme precipitation, were examined in this study under present and future climate conditions.

2. Model description and configuration

In this study, CESM version 1.0 was used for global climate simulations. CESM 1.0, the state-of-the-art global climate model developed by the NCAR, is composed of four major components including atmosphere, ocean, land surface and sea ice. The atmospheric component CAM4, described earlier, uses the finite-volume (FV) dynamical core [14] with a horizontal latitude/longitude grid of 0.9° × 1.25° and 26 vertical layers. The land component is the Community Land Model (CLM4) [25], which incorporates the effects of CO_2 and nitrogen on plant fertilization and growth [26]. The ocean component is the Parallel Ocean Program version 2 (POP2) [27], with dramatic improvement in the thermocline structure and SST [28] over POP version 1.4 [29, 30] used in CCSM3 and PCM. The sea ice component uses the code from the Los Alamos National Laboratory Sea Ice Model, version 4 (CICE4) [31], on which substantial improvement has been achieved over new radiative transfer scheme and aerosols [32].

The latest version of regional climate model WRF 3.2.1 [33] was used in the regional climate simulations. The most widely used physics in US simulation domain was selected in this study, including: the new Kain–Fritsch convective parameterization [13, 34–36], the single-moment 6-class microphysical scheme (WSM6) [12, 13, 36, 37], the Mellor–Yamada–Janjic planetary boundary layer (PBL) scheme [35, 38, 39] and the Noah land surface model [13, 35, 40]. For the shortwave and longwave radiation scheme, the rapid radiative transfer model (RRTM), widely used in US WRF simulations [35, 41], can reproduce highly accurate line-by-line results, while improved efficiency was provided by the new scheme RRTM for GCMs (RRTMG) [42, 43]. Thus, RRTMG was used in this study. Since there are no cumulus parameterization schemes suitable for the 4 km × 4 km scales at present [44], no convective parameterization scheme was used for the 4 km × 4 km domain.

Three domains were designed for WRF simulations, as is shown in figure 1. The outer domain (D1) with a resolution of 36 km × 36 km is centered at 97°W, 40°N. The second domain (D2) is 12 km × 12 km and covers most of North

---

[4] www.iiasa.ac.at/web-apps/tnt/RcpDb/dsd?Action=htmlpage&page=about.

[5] www.ncdc.noaa.gov/billions/.

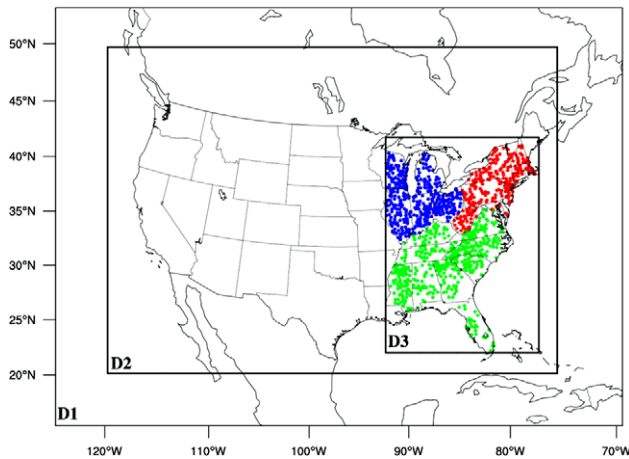[6] http://cred.be/sites/default/files/PressConference2010.pdf.

Figure 1. WRF simulation domains: D1 (36 km × 36 km resolution), D2 (12 km × 12 km) and D3 (4 km × 4 km). The points represent NCDC US COOP network station observation points in three regions: northeast (red color), eastern Midwest (blue color) and southeast (green color).

America and the inner domain (D3) with a high resolution of 4 km × 4 km, shown in figure 1. The boundary between nest and mother domain is suggested[7] at least 5 grid points, and to ensure enough buffer zone, 10 grids or more are used in the domain design for this study. D3 can be divided to three sub-regions based on the definition of the US Global Change Research Program (USGCRP)[8]: northeast (red color), eastern Midwest (blue color) and southeast (green color) regions. The colored points in each state represent the observational data point over quality controlled National Climatic Data Center (NCDC) US COOP network station observations (referred to as NCDC)[9], which will be used for model evaluations in section 3. This dataset is selected to evaluate extreme events; daily maximum temperature, daily minimum temperature and daily precipitation are required for the evaluations. The observational data has been well documented by Meehl *et al* [45]. This domain size is significant and computationally intensive, but the high computational effort for these regions is justified since the regions contain large populations which may be affected by climate change. The main purpose of this study is high resolution downscaling; the regional climate analysis will mainly focus on the downscaled 4 km × 4 km eastern US.

For the CMIP5, present climate simulations and four future climate RCP (RCP 2.6, RCP 4.5, RCP 6.0 and RCP 8.5) scenarios were designed. The present climate simulations with CESM are from 1850 to 2005 and the RCP scenarios are from 2005 to 2100. The analysis of global climate simulations were well documented by Meehl *et al* [24]. Considering the limited computational resources in this regional high resolution downscaling study, a four year period (2001–4) was selected to represent present climate and one RCP scenario

(RCP 8.5 [46]) was used to illustrate future climate conditions from 2057–9. For both present and future climate simulations, one month spin-up period was applied before both modeling periods in order for the model to reach equilibrium, as suggested by previous studies [47, 48]. Among the four RCP scenarios, RCP 8.5 projects the most intensive fossil fuel emissions, which is comparable [24] to the Special Report on Emissions Scenarios (SRES) A1FI [49] scenario.

3. Dynamical downscaling methodology

At each three-hour interval, CESM outputs were dynamically used to establish boundaries for the outer WRF domain simulations. A number of variables, including both surface and three-dimensional variables, are required for dynamical downscaling. Most of the variables are extracted in the CAM4 outputs, while soil moisture and soil temperature are taken from the CLM4 history outputs.

Surface variables are horizontally interpolated from CESM (CAM4 and CLM4, 0.9° × 1.25° spatial resolution in latitude/longitude) to WRF simulation domains. In this step, the WRF Preprocessing System (WPS) is used to interpolate CESM output into WRF domains. Physics are not involved in this process, and theoretically, the outputs from CESM and WPS should show similar spatial patterns or integrity. This phenomenon was observed for most of the downscaled variables (not shown) except for skin temperature.

Figure 2 shows the spatial patterns for skin temperature in the first time step (0:00 on 1 January 2001). Figure 2(a) is extracted from CESM outputs and figure 2(b) is from WPS. Between these two plots, significant differences are apparent near the Great Lakes region. When horizontally interpolating typical variables (other than skin temperature) from CESM outputs, WPS uses the nearest 16 grids in distance-weighted interpolation. However, the skin temperature in water area uses the nearest temperature in water (sea surface temperature) reflected by the land/sea mask in CAM4. The land/sea mask of Great Lakes region was land in CAM4, thus, interpolation occurs using the nearest sea surface temperature to the right side (green contour in figure 2(b)). To achieve consistent skin temperature between CAM4 and WPS, the land/sea mask from CAM4 in the Great Lakes region has been changed to the same as ocean areas. After the modification, the spatial pattern of skin temperature from WPS (figure 2(c)) shows consistent temperature distributions with CESM (figure 2(a)) in the Great Lakes region. A sensitivity test showed that the improved skin temperature could reduce the bias of 2 m air temperature between WRF and CESM as high as 10 °C for the Great Lakes region.

4. State-level extreme events evaluations of dynamical downscaling

Before investigating the extreme events such as heat waves and extreme precipitation in a future climate, we first evaluated how well WRF predicts the extreme events (by comparing to observations) and how much improvement can be gained from the high resolution downscaling.

---

[7] www.mmm.ucar.edu/mm5/documents/MM5_tut_Web_notes/TERRAIN/terrain.htm.

[8] http://globalchange.gov/publications/reports/scientific-assessments/us-impacts/regional-climate-change-impacts.
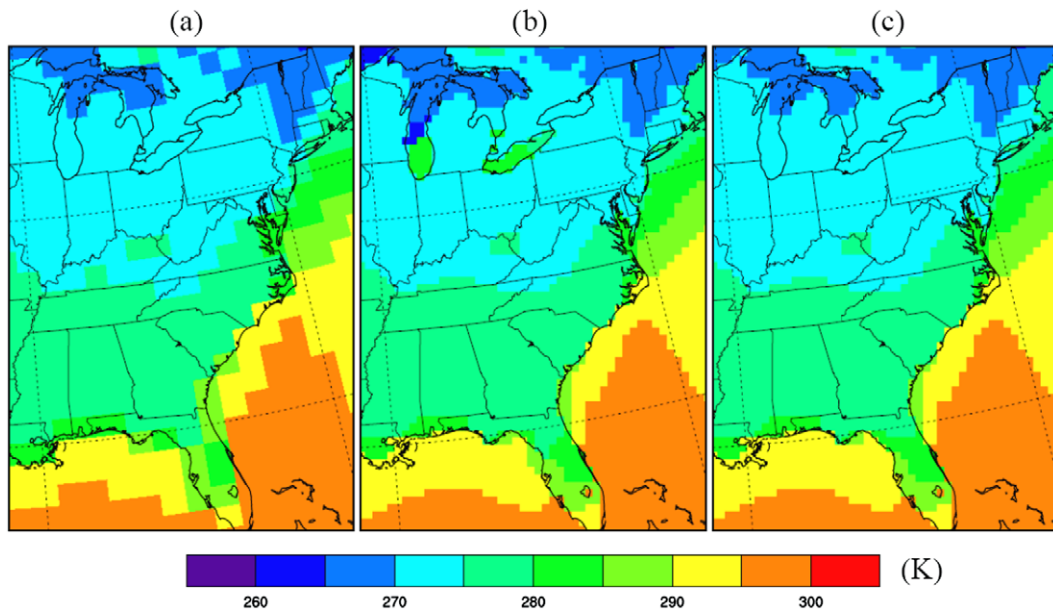
[9] http://dss.ucar.edu.

Figure 2. Skin temperature comparisons: (a) CESM; (b) WPS output without changing land use type; (c) WPS output after modifying the land/sea mask.

4.1. Evaluations of heat wave intensity, duration and frequency

We studied three key parameters of heat waves at an annual basis: intensity, duration and frequency. Heat wave intensity (°C) is defined as the highest three continuous nighttime minima [50]. Heat wave duration (number of days during a heat wave) and frequency (number of heat wave events per year) are based upon two thresholds, T1 and T2, of daily maximum temperature. We define a heat wave as the longest continuous period satisfying three criteria: (a) the maximum daily temperature remained T1 or higher for at least three continuous days, (b) the mean daily maximum temperature is higher or equal to T1, and (c) in each day, the daily maximum temperature is no lower than T2 [23, 51]. T1 and T2 are taken as the 97.5th and 81st percentiles [51] of daily maximum temperature at present climate (2001–4) based on previous studies. Considering model dependency of these percentiles, the thresholds were applied to CESM, WRF and NCDC observational data, respectively. In other words, the same percentile thresholds (97.5th and 81st) in these three datasets correspond to different temperatures. Theoretically, it is the best to get the same 97.5th or 81st percentile among CESM, WRF and NCDC. However, this desirable condition hardly exists for climate studies. Each model has its own probability (cumulative) distribution of daily maximum temperature, thus the evaluation of the distributions was first discussed in the supplementary material (available at stacks.iop.org/ERL/7/044025/mmedia) (section 1). Overall, the cumulative distributions of daily maximum temperature in both CESM and WRF fit NCDC fairly well (supplementary material available at stacks.iop.org/ERL/7/044025/mmedia). Although biases exist in the thresholds, they are more likely to exist in the heat wave duration and frequency as well. Thus, by using thresholds from each dataset and further evaluate heat

wave duration and frequency, we can find out whether regional climate model has the skill to improve the extreme weather events predictions compared with global climate model. In addition, there are only limited observation points in NCDC (1065 points in the eastern US), and the high resolution WRF domain (4 km × 4 km) contains more than 100 000 grid points. If only using thresholds from NCDC, a majority of grid points in WRF will be interpolated from NCDC. In this case, the large spatial variations and representation achieved in the high resolution simulations cannot be fully taken advantage of. Thus, the temperature threshold from each dataset is used in this study. For future heat waves in CESM and WRF simulations, the same temperature thresholds as present climate were retained in order to characterize the changes between the present and future climate.

The heat wave parameters were first evaluated for each year, and then the four year (2001–4) mean was calculated and used in the following analysis. The heat wave intensity, duration and frequency were calculated from CESM outputs, WRF outputs and NCDC data. The evaluations were based on the NCDC observations covering 23 states in the eastern US and all the 1098 observational sites (figure 1) were used for point–point comparisons. Heat waves at each point in the NCDC network and the corresponding grid in CESM/WRF were determined separately. State means were then calculated and are compared in table 1. The 23 states can be divided into three regions (shown in figure 1): northeast, eastern Midwest and southeast. The evaluations of regional mean, derived from arithmetic mean using stations points for NCDC and the corresponding model points for CESM and WRF within each region, are bolded in table 1.

Following each of the regional means is the evaluation for the states belonging to the region. A *t*-test ($\alpha = 0.05$) was performed to determine the statistical significance of the improvement in WRF over CESM. From table 1, there are

Table 1. Evaluations of heat wave intensity, duration and frequency.

Regions/States	Heat wave intensity (°C)				Heat wave duration (days/event)				Heat wave frequency (events yr^{-1})			
	NCDC	CESM-NCDC	WRF-NCDC	%[a]	NCDC	CESM-NCDC	WRF-NCDC	%[a]	NCDC	CESM-NCDC	WRF-NCDC	%[a]
Northeast region	**20.82**	**1.55**	**1.17**	**25**	**5.62**	**1.27**	**-0.41**	**68**	**1.44**	**-0.76**	**-0.29**	**62**
New Hampshire	19.22	2.21	1.91	14	5.42	-0.09	-1.01	-91	1.53	-1.05	-0.35	67[b]
Vermont	19.23	1.30	1.49	-13	6.20	1.36	-0.83	39	1.41	-0.91	-0.44	52
Massachusetts	21.70	2.33	0.99	58[b]	5.28	0.70	-0.46	34[b]	1.26	-0.34	-0.27	21
Connecticut	21.28	1.44	0.99	31	5.55	-1.10	-1.07	3	1.41	-0.66	-0.27	59
New York	20.16	1.12	0.78	30[b]	5.97	-0.73	-0.59	19[b]	1.49	-0.91	-0.57	37[b]
Pennsylvania	19.93	1.65	1.01	39[b]	5.92	1.53	-1.13	26[b]	1.5	-0.71	-0.17	76[b]
New Jersey	22.17	1.75	1.48	15	5.47	0.73	-0.15	79	1.45	-0.93	-0.22	76[b]
Maryland	23.24	1.01	1.50	-33	6.27	4.34	-0.40	91[b]	1.36	-0.53	-0.14	74
West Virginia	20.43	1.18	0.38	68[b]	4.50	4.66	1.96	58[b]	1.54	-0.78	-0.15	81[b]
Eastern Midwest Region	**21.31**	**2.51**	**1.15**	**54**	**5.00**	**3.98**	**1.24**	**69**	**1.42**	**-0.23**	**-0.20**	**13**
Wisconsin	20.86	2.21	1.04	53[b]	5.13	2.97	1.18	60[b]	1.31	-0.26	-0.39	-33
Michigan	20.18	2.47	1.93	22[b]	4.92	3.00	1.14	62[b]	1.4	-0.08	-0.07	13
Illinois	22.46	3.36	1.23	63[b]	4.97	5.30	1.25	76[b]	1.43	-0.24	0.15	38
Indiana	21.94	2.53	0.89	65[b]	5.00	5.95	1.29	78[b]	1.51	-0.48	-0.21	56
Ohio	21.12	1.98	0.68	66[b]	4.98	2.70	1.36	50[b]	1.44	-0.09	-0.18	-50
Southeast region	**22.58**	**1.47**	**0.83**	**43**	**6.51**	**3.67**	**1.98**	**46**	**1.34**	**-0.34**	**-0.24**	**28**
Kentucky	22.28	1.82	0.57	69[b]	6.56	6.15	1.93	69[b]	1.26	-0.45	-0.01	98[b]
Virginia	20.98	2.17	1.28	41[b]	6.20	3.50	2.13	39[b]	1.33	-0.39	-0.19	51
Tennessee	22.08	1.62	0.93	43[b]	6.59	5.97	3.16	47[b]	1.26	-0.26	-0.21	19
North Carolina	21.61	1.69	1.09	36[b]	6.82	1.90	0.93	36[b]	1.36	-0.2	-0.22	-9
Mississippi	23.18	1.66	0.79	52[b]	5.86	4.46	3.55	52[b]	1.4	-0.33	-0.39	-15
Alabama	22.78	1.04	1.10	-5	5.06	3.53	2.34	20	1.47	-0.59	-0.49	17
Georgia	22.10	1.11	1.06	5	7.63	2.76	0.81	71	1.12	-0.09	-0.1	-10
South Carolina	23.04	1.03	0.71	31[b]	7.78	3.76	1.43	62	1.18	-0.35	-0.08	77
Florida	25.15	1.13	-0.03	97[b]	6.05	1.04	1.58	-34	1.64	-0.37	-0.48	-23

[a] Numbers without sign: indicating bias percentage improvement in WRF over CESM in comparison to NCDC data, with formula of ($|$CESM-NCDC$|$ − $|$WRF-NCDC$|$)/$|$CESM-NCDC$|$. Numbers with negative sign: indicating bias in CESM is smaller than WRF in comparison to NCDC, with formula of ($|$CESM-NCDC$|$ − $|$WRF-NCDC$|$)/$|$WRF-NCDC$|$.
[b] Statistical significance of *t*-test ($\alpha = 0.05$).

16 and 14 states showing statistically significant improvement for heat wave intensity and duration, respectively. However, only 6 states show statistical improvement for heat wave events, mainly due to the small number of heat wave events. The improvement in WRF for heat wave intensity is primarily contributed by more realistic topography, while the improvement for heat wave duration and frequency indicates better skill in regional climate models. Among the states with statistically significant improvement in WRF over CESM, the greatest improvements include: heat wave intensity in Florida (97%), heat wave duration in Maryland (91%) and heat wave frequency in Kentucky (98%). For those states that CESM achieves lower bias than WRF (numbers with negative sign), the performance differences between CESM and WRF are not statistically significant. Thus, by taking advantage of high resolution topography and land use information, dynamical downscaling statistically improves, or at least performs similarly to, CESM for the heat wave reproducing over the eastern US.

4.2. Evaluations of precipitation and extreme precipitation

A rainy day is defined as a day when the daily precipitation totals at least 1 mm [52]. In the current analysis, extreme precipitation is defined as the 95th percentile of all the rainy days [52, 53]. The 95th percentile threshold is calculated as the mean of each year's 95th percentile precipitation from 2001 to 2004 for each dataset from CESM, WRF and NCDC [10, 53]. Similar as the explanation in section 4.1, using the 95th percentile thresholds from each dataset not only take advantage of high regional resolution, but also indicate the skill of regional climate model in predicting extreme weather events. The determination of 95th percentile threshold is location dependent, so no fixed value is used in this definition. The following indices were used for the evaluations:

- Total extreme precipitation (mm yr^{-1}): annual total of extreme daily precipitation amounts.
- Annual extreme events (days yr^{-1}): frequency of extreme daily precipitation events.
- Daily extreme precipitation (mm d^{-1}): annual mean rate of extreme daily precipitation, which is calculated as the total amount of annual extreme precipitation divided by total annual extreme precipitation days.

The probability distributions of precipitation on rainy days are shown in figure 3 for each of the 23 states in the eastern US. In addition, the probability distributions of daily precipitation 40 mm or more is magnified and plotted in the middle of each plot. The value of 40 is significant because in the majority of the states, daily precipitation values of 40 mm or more account for less than 5% of rainy days, which is considered extreme precipitation. Annual extreme precipitation totals were also evaluated and listed in the upper portion of each plot.

WRF-simulated precipitation probability distributions are in closer agreement with NCDC observations than CESM (figure 3). The CESM tends to yield larger percentages of rainy days with daily precipitation from 1 to 5 mm, but lower percentages with daily precipitation of 10 mm or more. The probability distributions of extreme precipitation in WRF agree more closely with NCDC data, while CESM data substantially underestimate the frequency of extreme precipitation. In the northeast, six states (Massachusetts, New York, Pennsylvania, New Jersey, Maryland and West Virginia) have improvement over 70% in both total extreme precipitation and extreme precipitation days in WRF over CESM. Three states in the eastern Midwest (Wisconsin, Illinois and Indiana) and five states in the southeast (Kentucky, Virginia, North Carolina, Georgia and South Carolina) have similarly high improvement in WRF over CESM. However, a few exceptions exist. For instance, WRF overpredicts extreme precipitation in New Hampshire and Connecticut, and the amount by which precipitation is over predicted is larger than the under predicted amount in CESM. In parts of the southeast, such as in Florida, both CESM and WRF under predict the extreme precipitation, but WRF tends to capture more extreme events. This phenomenon indicates that dynamical downscaling with WRF has the capability of reproducing extreme precipitation better than CESM. However, more than 20 hurricane events[10] occurred during 2001–4, which is possibly not captured well by either CESM or WRF, resulting in less extreme precipitation events in both models compared to NCDC. Overall, 32–33% improvement was achieved in WRF downscaled outputs. In addition, the dynamical downscaling not only captures better probability distributions of extreme precipitation, but also results in improvement of the reproducing in both annual extreme precipitation amount and precipitation days.

5. Increasing trends of state-level extreme events by the end of 2050s

5.1. Increasing trends of heat wave intensity, duration and frequency

The spatial distributions of heat wave intensity, duration and frequency at present (2001–4) and future climate (RCP 8.5, 2057–9) are shown in figure 4 and the region/state means are shown in table 2. First, we performed a *t*-test ($\alpha = 0.05$), and found mean RCP85 outputs is statistically greater than present climate for heat wave intensity, duration and frequency except heat wave duration in Tennessee.

Figure 4(a) shows, at present, the heat wave intensity is higher in the southeast (mostly higher than 23 °C) than the northeast and the eastern Midwest. A few hot spots, indicating higher heat wave intensity, are located in the megacities, such as Chicago and Detroit in the eastern Midwest, Washington DC, Philadelphia and New York City in the northeast, Memphis and Atlanta in the southeast. The urban heat island effects were captured by regional climate simulations, mainly contributing by the higher resolution landscape in Noah land surface model in WRF than CLM4. In addition to the

---

[10] http://en.wikipedia.org/wiki/List_of_Florida_hurricanes_%282000%E2%80%93present%29#2001.
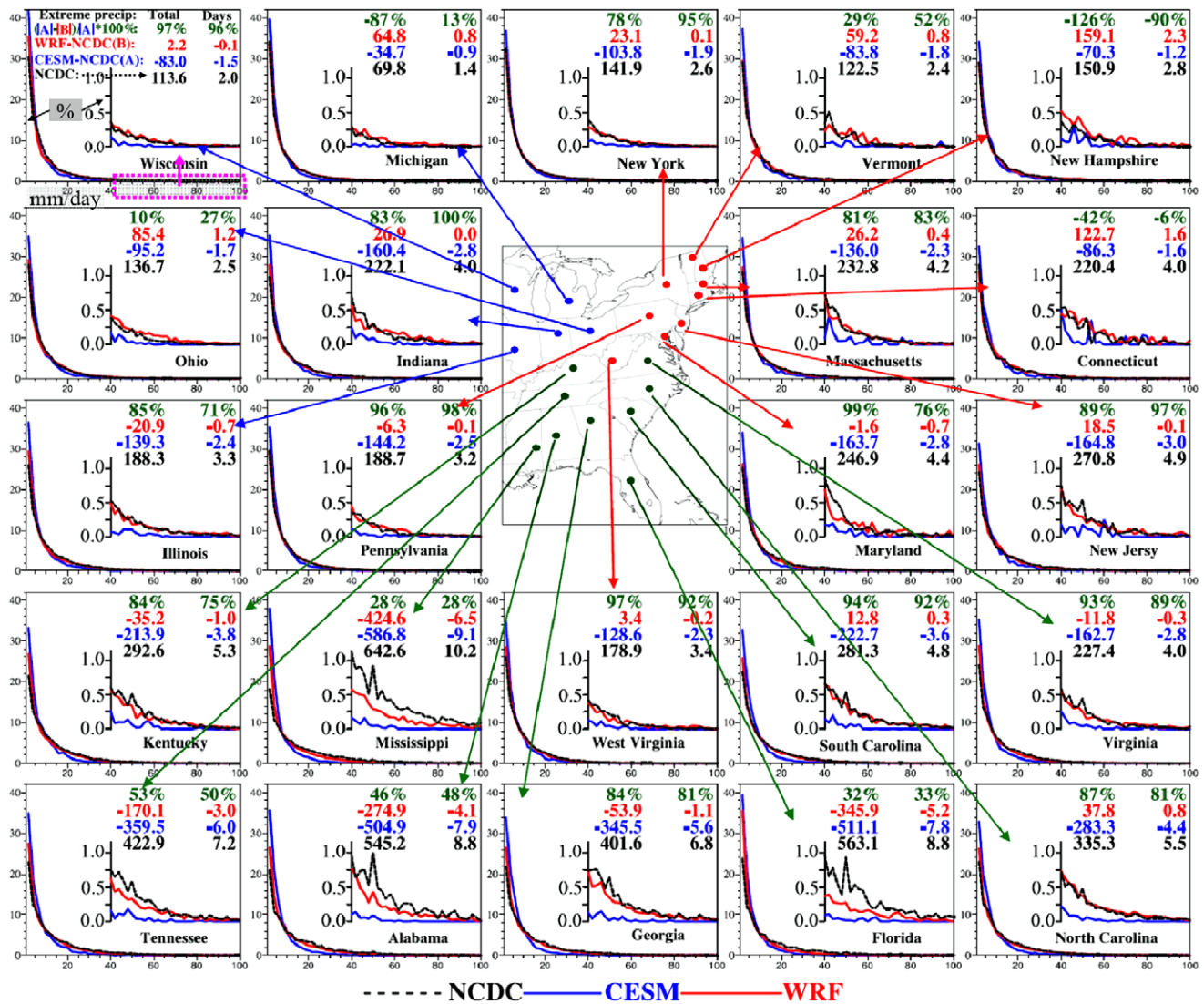
Figure 3. Probability distributions of precipitation from NCDC, CESM and WRF outputs. The probability distributions of daily precipitation 40 mm or more (extreme precipitation) is zoomed in and plotted in the middle of each plot. Total annual extreme precipitation amounts and days were listed in the upper portion of each plot. The numbers on the left represent total annual extreme precipitation, with NCDC in black, bias in CESM (CESM-NCDC) in blue, bias in WRF (WRF-NCDC) in red and the bias reduction in WRF over CESM $((|\text{CESM-NCDC}| - |\text{WRF-NCDC}|)/(|\text{CESM-NCDC}|) \times 100\%$, in green); the numbers on the right are similar to the left but apply to the annual extreme precipitation days.

state-level studies, 20 cities in the eastern US (top 50 by population in US) were also selected to investigate these urban heat waves (extreme precipitation as well) and more intense heat waves and extreme precipitation was found in future climate for majority of these cities (details are discussed in the supplementary material available at stacks.iop.org/ERL/7/044025/mmedia).

By the end of 2050s (2057–9), the severity of heat waves increases in most of the areas in the eastern US (figures 4(b) and (c)). Again, the southeast still shows highest intensity; however, the highest increase occurs in the northeast (figure 4(c)), reaching 3–5 °C, pushing the northeast to the current conditions in the southeast. In the northeast, six states (New Hampshire, Vermont, New York, Pennsylvania, New Jersey and Maryland) have an increase of higher than 3 °C, with the highest increase occurring in the state of New York.

Figure 4(d) shows, at present, the heat wave duration is similar in the northeast and eastern Midwest, about 4 days/event, while in southeast it could reach more than 7 days/event. By the end of 2050s, the heat wave duration decreases in the center areas (Tennessee, Mississippi and Alabama) of southeast, while the northeast and eastern Midwest show an increase of 2 days/event event on average (figures 4(e) and (f)). The decrease of heat wave duration does not necessarily mean the annual total heat wave days decrease. Particularly, in this case, for Tennessee, Mississippi and Alabama, even though the heat wave duration slightly decreases in future, the annual total heat wave days are 21.2, 12.9 and 19.8 in RCP 8.5, while they are only 6.3, 6.3 and 5.6 at present. There is about 1 event yr^{-1} at present from figure 4(g), while 5 or more events could occur in the northeast, eastern Midwest and Florida by the end of the 2050s under the RCP 8.5 scenario (figures 4(h) and (i)). Combining
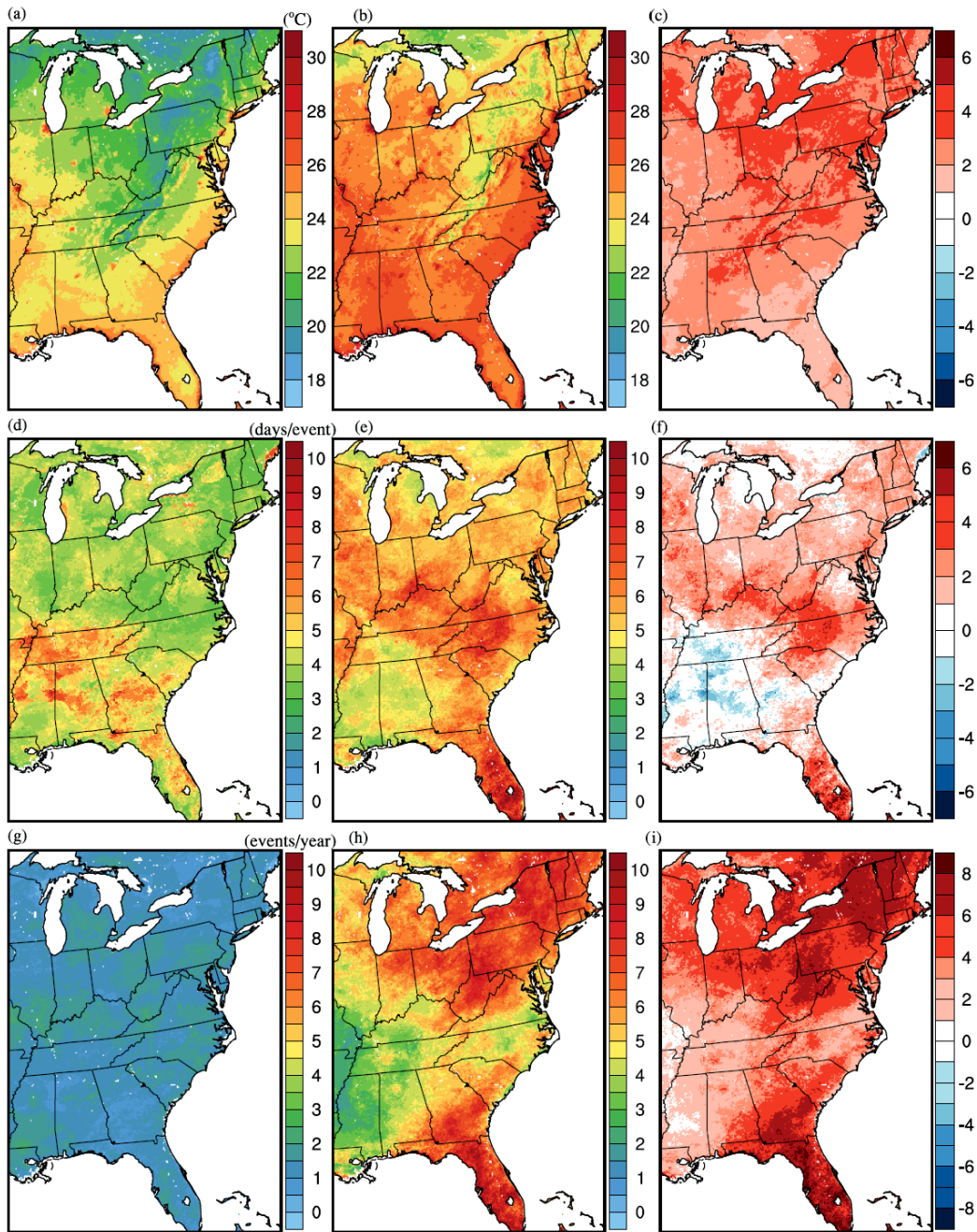
Figure 4. The spatial distributions of heat wave intensity, duration and frequency at present (2001–4) and future climate (RCP 8.5, 2057–9): (a) four year average of heat wave intensity at present climate (2001–4), (b) three year average of heat wave intensity at future climate under RCP 8.5, (c) the differences of heat wave intensity between RCP 8.5 and present climate (RCP 8.5—present climate), (d)–(f) are similar as (a)–(c), but applies to heat wave duration, (g)–(i) are similar as (a)–(c) as well, but applies to heat wave frequency.

the heat wave duration and frequency, the total heat wave days in the northeast and eastern Midwest would be higher than southeast.

5.2. Increases in the state-level extreme precipitation

At present (figure 5(a) and table 3), the total extreme precipitation in the northeast and southeast is larger than the eastern Midwest. The highest annual extreme precipitation, 371.0 mm, occurs in Connecticut. By the end of 2050s, while scattered decreases in extreme precipitation exist, most areas

show increasing patterns, as seen in figures 5(b) and (c). As shown in figure 5(c), the largest increase (dark green) takes place mainly in the coastal states, including New Hampshire, New Jersey, North Carolina, South Carolina, Georgia and Alabama, with an increase of around 150 mm yr^{-1} (table 3). From table 3, almost half of the states have a total extreme precipitation increase of more than 35%, including five states in the northeast (New Hampshire, Vermont, Massachusetts, New Jersey and Maryland), two in the eastern Midwest (Illinois and Indiana) and four in the southeast (North

Table 2. Heat wave intensity, duration and frequency.

Regions/states	Heat wave intensity (°C)			Heat wave duration (days/event)			Heat wave frequency (events/yr)		
	Present	RCP 8.5	RCP 8.5—Present	Present	RCP 8.5	RCP 8.5—Present	Present	RCP8.5	RCP 8.5—Present
Northeast region	**21.81**	**24.85**	**3.05**	**3.61**	**5.53**	**1.92**	**1.24**	**7.03**	**5.79**
New Hampshire	21.16	24.23	3.07	3.22	5.35	2.13	1.29	7.41	6.12
Vermont	20.84	24.02	3.18	3.37	5.35	1.98	1.15	7.94	6.79
Massachusetts	22.21	25.05	2.84	3.60	5.47	1.87	1.02	7.13	6.11
Connecticut	22.45	25.43	2.98	3.68	5.71	2.03	1.24	6.53	5.29
New York	20.84	24.08	3.24	3.78	5.32	1.54	0.96	7.65	6.69
Pennsylvania	20.97	24.16	3.19	3.85	5.48	1.63	1.33	7.26	5.93
New Jersey	23.44	26.55	3.11	3.59	5.49	1.90	1.36	6.26	4.90
Maryland	23.26	26.33	3.07	3.91	5.67	1.76	1.34	5.89	4.55
West Virginia	21.08	23.82	2.74	3.53	5.96	2.43	1.45	7.16	5.71
Eastern Midwest Region	**22.26**	**25.05**	**2.78**	**3.86**	**5.65**	**1.78**	**1.23**	**5.57**	**4.34**
Wisconsin	21.63	24.61	2.98	3.64	5.63	1.99	0.97	5.23	4.26
Michigan	21.70	24.62	2.92	3.96	5.00	1.04	1.20	5.78	4.58
Illinois	23.48	25.74	2.26	3.97	5.94	1.97	1.32	4.50	3.18
Indiana	22.72	25.28	2.56	3.87	5.87	2.00	1.37	5.66	4.29
Ohio	21.79	24.99	3.20	3.88	5.80	1.92	1.30	6.70	5.40
Southeast region	**23.53**	**25.99**	**2.46**	**4.55**	**5.78**	**1.23**	**1.25**	**5.02**	**3.77**
Kentucky	22.80	25.54	2.74	4.22	6.28	2.06	1.41	4.48	3.07
Virginia	22.50	25.43	2.93	3.70	6.00	2.30	1.38	5.38	4.00
Tennessee	23.00	25.69	2.69	5.47	5.46	−0.01	1.16	3.88	2.72
North Carolina	23.27	26.06	2.79	3.82	6.45	2.63	1.35	4.71	3.36
Mississippi	23.99	26.21	2.22	4.70	4.41	−0.29	1.35	2.93	1.58
Alabama	23.80	26.34	2.54	4.96	4.57	−0.39	1.12	4.33	3.21
Georgia	23.74	25.92	2.18	4.98	5.66	0.68	1.02	6.19	5.17
South Carolina	23.98	26.32	2.34	4.41	6.08	1.67	1.33	5.46	4.13
Florida	24.67	26.38	1.71	4.66	7.11	2.45	1.09	7.81	6.72

Carolina, Alabama, Georgia and South Carolina). However, some inland regions show decreasing extreme precipitation (figure 5(c)), including part of New York, Pennsylvania, Ohio and West Virginia, Illinois and Tennessee. Wisconsin is the only state with overall decreasing mean extreme precipitation by the end of 2050s (18.3 mm less per year from table 3).

Daily extreme precipitation ranges from 40 to 60 mm d^{-1} at present (figure 5(d)). By the end of 2050s (figures 5(e) and (f)), smaller increases occur in the northeast and eastern Midwest, while larger increases occur in the southeast. As shown in figures 5(c) and (f), the southeast has the largest increase in both daily extreme precipitation and annual extreme precipitation days, while the eastern Midwest shows less increase. At present, about 4–6 days per year have extreme precipitation (figure 5(g)), while 8–12 days could occur per year in large areas of the northeast and southeast by the end of 2050s (figure 5(h)), indicating the extreme precipitation days could increase to twice as many as present conditions (figure 5(i)).

In addition to the extreme precipitation days, we also compared the percentage change of annual extreme precipitation to annual total precipitation. We found at present, the extreme precipitation accounts for 25% (West Virginia) to 30% (Wisconsin) of annual total precipitation; by the end of 2050s, these percentage ranges from 27% in West Virginia to 39% in Illinois, with a mean increase of 7% across the eastern US. The three largest increases (more than 10%) occur in New Hampshire (13%), Alabama (12%) and Illinois (11%). At present, Wisconsin has the largest percentage in

extreme precipitation (30%). However, it is the only state that is projected to have a slight decrease in extreme precipitation percentage (about 1%), while all other states show increasing trends in extreme precipitation percentage (3%–13%).

6. Conclusions

The regional climate dynamical downscaling technique has been successfully applied to CESM results for the RCP 8.5 climate change scenario to generate high resolution climate outputs. When conducting dynamical downscaling, one should examine spatial patterns to determine whether consistency between models exists. In this study, the inconsistency in skin temperature between CESM and WRF was corrected by modifying the land/sea mask from CESM. The downscaling using CCSM has been widely studied, but no one has reported inconsistency of skin temperature so far. We recommend downscaling studies using either CCSM/CESM or other global climate models compare the spatial patterns between global climate models and WPS outputs before producing WRF simulations.

The extreme events evaluations of CESM and WRF in comparison to NCDC network prove that WRF is more capable than CESM in reproducing local extreme events. The percentage improvement could reach as high as 97% in Florida for heat wave intensity, 91% in Maryland for heat wave duration, 98% in Kentucky for heat wave frequency (table 1), more than 95% in Wisconsin and Pennsylvania
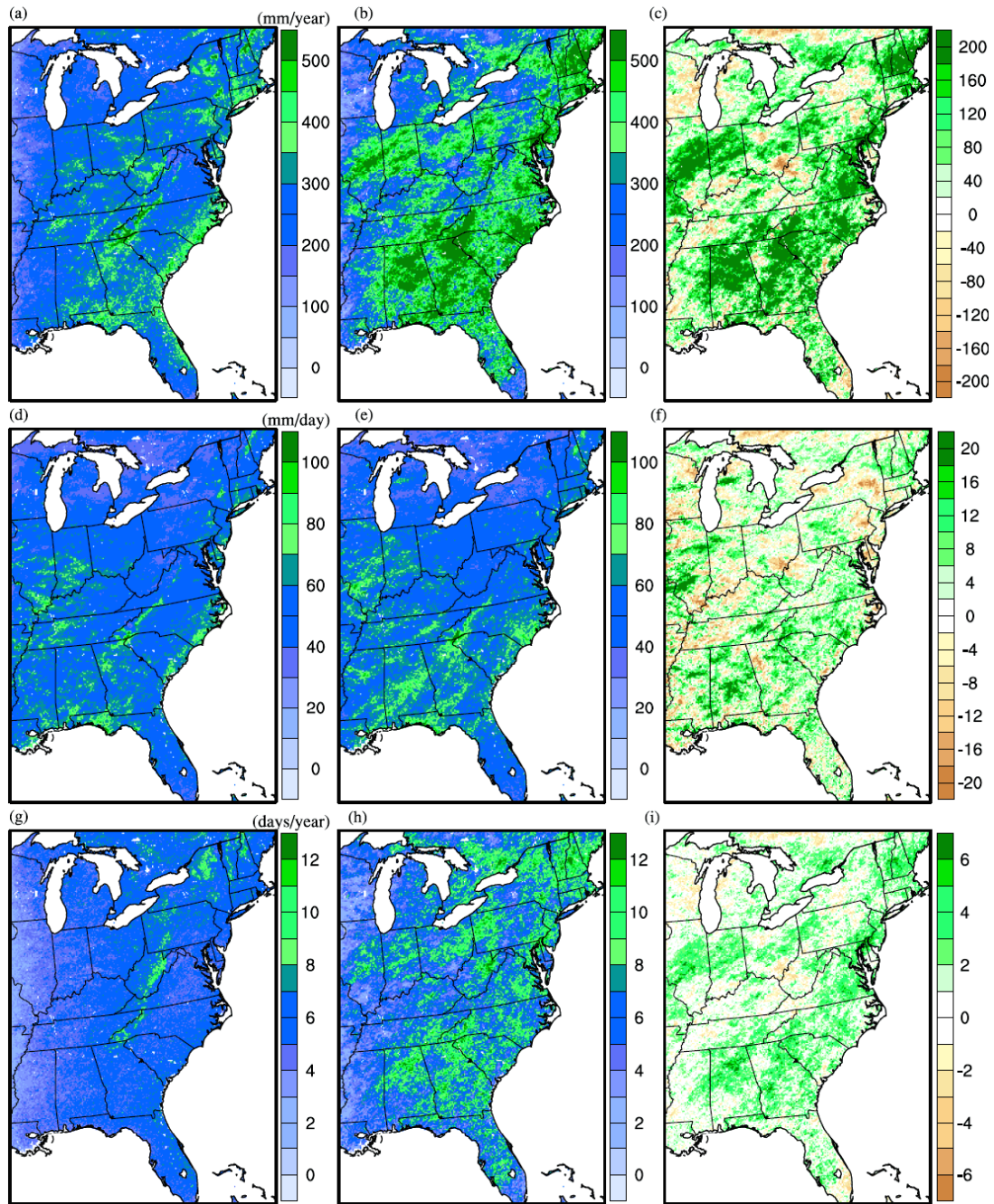
Figure 5. The spatial distributions of total extreme precipitation (a)–(c), daily extreme precipitation (d)–(f) and annual extreme events (g)–(i) at present (2001–4), future climate (RCP 8.5, 2057–9) and changes in future (RCP 8.5–Present).

for both annual extreme precipitation and annual extreme events (figure 3). Thus, by taking advantage of high resolution topography, land use information and the skill of regional climate model, the dynamical downscaling dramatically improves the heat wave and extreme precipitation reproducing over the eastern US. Thus, the coarse resolution global climate model results may not be suitable for regional/local extreme climate studies.

The RCP 8.5 scenario was used as an example to study the future climate in 2057–9 compared to present climate in 2001–4. By the end of 2050s, the heat waves become more severe in most regions of the eastern US. The increases in the

northeast and eastern Midwest are more than the southeast, which reduces the severity of differences among the north and south regions. It is an indicator that northeast and eastern Midwest may suffer more resulting from a steeper increase in the severity of heat waves. The total annual extreme precipitation in both the northeast and southeast have a mean increase of 35% or more, suggesting a greater risk of flooding in future climate conditions. Considering both heat waves and extreme precipitation, the northeast region shows the largest increases. Thus, it is important that the northeast take actions to mitigate the impact from climate change in the next several decades.

Table 3. Total extreme precipitation, daily extreme precipitation and annual extreme events. (Note: A *t*-test ($\alpha = 0.05$) was performed, and by the end of 2050s, the extreme precipitation is statistically more intense than present climate except for daily extreme precipitation in Ohio.)

Regions/states	Total extreme precipitation (mm yr^{-1})			Daily extreme precipitation (mm day^{-1})			Annual extreme events (days yr^{-1})		
	Present	RCP8.5	RCP 8.5—Present	Present	RCP8.5	RCP 8.5—Present	Present	RCP8.5	RCP 8.5—Present
Northeast region	**308.7**	**416.1**	**107.3**	**51.1**	**52.6**	**1.5**	**6.1**	**7.9**	**1.8**
New Hampshire	324.4	537.6	213.3	49.7	55.7	6.0	6.5	9.6	3.1
Vermont	286.2	415.7	129.5	43.1	46.7	3.6	6.5	8.8	2.2
Massachusetts	328.5	454.3	125.8	54.5	56.7	2.1	6.1	8.1	2.1
Connecticut	371.0	444.3	73.3	61.4	60.7	−0.8	6.2	7.4	1.3
New York	292.5	332.5	40.0	45.7	44.9	−0.8	6.4	7.4	1.0
Pennsylvania	290.8	359.8	69.0	47.9	49.6	1.6	6.1	7.3	1.2
New Jersey	307.7	458.4	150.7	57.8	56.9	−0.9	5.4	8.1	2.8
Maryland	272.9	402.3	129.3	52.9	54.3	1.4	5.2	7.5	2.3
West Virginia	304.8	339.5	34.8	46.7	48.3	1.5	6.6	7.2	0.6
Eastern Midwest Region	**235.2**	**293.8**	**58.7**	**50.6**	**52.0**	**1.5**	**4.7**	**5.6**	**0.9**
Wisconsin	182.9	164.7	−18.3	44.5	43.5	−1.0	4.0	3.8	−0.2
Michigan	217.8	254.0	36.1	42.1	44.2	2.2	5.2	5.8	0.6
Illinois	208.0	322.9	114.9	55.6	60.0	4.4	3.7	5.3	1.6
Indiana	277.8	386.8	109.1	58.5	60.1	1.7	4.8	6.5	1.7
Ohio	289.3	340.8	51.5	52.1	52.3	0.2	5.6	6.6	1.1
Southeast region	**294.6**	**405.0**	**110.4**	**56.8**	**60.6**	**3.9**	**5.2**	**6.7**	**1.5**
Kentucky	287.6	329.8	42.3	55.6	57.3	1.7	5.2	5.8	0.5
Virginia	262.0	388.2	126.3	50.2	54.5	4.4	5.2	7.1	1.9
Tennessee	293.2	365.7	72.5	57.8	59.4	1.6	5.1	6.2	1.1
North Carolina	338.1	477.7	139.6	59.3	64.6	5.3	5.7	7.4	1.7
Mississippi	226.0	286.8	60.8	57.4	60.4	3.0	4.0	4.8	0.8
Alabama	288.7	458.1	169.4	58.5	65.5	7.0	5.0	7.1	2.1
Georgia	330.4	490.7	160.4	59.3	63.6	4.3	5.6	7.8	2.2
South Carolina	323.1	482.4	159.4	57.9	62.9	5.0	5.6	7.7	2.1
Florida	302.1	365.4	63.3	55.0	57.7	2.7	5.6	6.4	0.8

Acknowledgments

References

[1] IPCC 2007 *Climate Change 2007: The Physical Science Basis. Contribution of Working Group I to the Fourth Assessment Report of the Intergovernmental Panel on Climate Change* ed S Solomon, D Qin, M Manning, M Marquis, K Averyt, M Tignor, H L Miller and Z Chen (Cambridge: Cambridge University Press)

[2] Caldwell P, Chin H-N S, Bader D C and Bala G 2009 Evaluation of a WRF dynamical downscaling simulation over California *Clim. Change* **95** 499–521

[3] Fowler H J, Blenkinsop S and Tebaldi C 2007 Linking climate change modelling to impacts studies: recent advances in downscaling techniques for hydrological modelling *Int. J. Climatol.* **27** 1547–78

[4] Diaz-Nieto J and Wilby R L 2005 A comparison of statistical downscaling and climate change factor methods: impacts on low flows in the River Thames, United Kingdom *Clim. Change* **69** 245–68

[5] Dickinson R E, Errico R M, Giorgi F and Bates G T 1989 A regional climate model for the western United States *Clim. Change* **15** 383–422

[6] Giorgi F 1990 Simulation of regional climate using a limited area model nested in a general circulation model *J. Clim.* **3** 941–63

[7] Giorgi F, Shields Brodeur C and Bates G T 1994 Regional climate change scenarios over the United States produced with a nested Regional Climate Model *J. Clim.* **7** 375–99

[8] Leung L R, Wigmosta M S, Ghan S J, Epstein D J and Vail L W 1996 Application of a subgrid orographic precipitation/surface hydrology scheme to a mountain watershed *J. Geophys. Res.* **101** 12803–17

[9] Podzun R, Cress A, Majewski D and Renner V 1995 Simulation of European climate with a limited area model. II: AGCM boundary conditions *Contrib. Atmos. Phys.* **68** 205–25

[10] Bell J L, Sloan L C and Snyder M A 2004 Regional changes in extreme climatic events: a future climate scenario *J. Clim.* **17** 81–7

[11] Salathé E P, Steed R, Mass C F and Zahn P H 2008 A high-resolution climate model for the U.S. Pacific Northwest: mesoscale feedbacks and local responses to climate change *J. Clim.* **21** 5708–26

[12] Pan L-L, Chen S-H, Cayan D, Lin M-Y, Hart Q, Zhang M-H, Liu Y and Wang J 2011 Influences of climate change on

California and Nevada regions revealed by a high-resolution dynamical downscaling study *Clim. Dyn.* **37** 2005–20

[13] Qian Y, Ghan S J and Leung L R 2010 Downscaling hydroclimatic changes over the western US based on CAM subgrid scheme and WRF regional climate simulations *Int. J. Climatol.* **30** 675–93

[14] Neale R B *et al* 2010 *Description of the NCAR Community Atmosphere Model (CAM 4.0)* (Boulder, CO: National Center for Atmospheric Research) p 194

[15] Neale R B, Richter J H and Jochum M 2008 The impact of convection on ENSO: from a delayed oscillator to a series of events *J. Clim.* **21** 5904–24

[16] Taylor K E, Stouffer R J and Meehl G A 2009 *A Summary of the CMIP5 Experiment Design* (http://pcmdi-cmip.llnl.gov/cmip5/experiment_design.html)

[17] Taylor K E, Stouffer R J and Meehl G A 2012 An overview of CMIP5 and the experiment design *Bull. Am. Meteorol. Soc.* **93** 485–98

[18] Moss R H *et al* 2010 The next generation of scenarios for climate change research and assessment *Nature* **463** 747–56

[19] Lott N and Ross T 2006 Tracking billion-dollar U.S. weather disasters *Bull. Am. Meteorol. Soc.* **87** 557–9

[20] Robine J-M, Cheung S L K, Le Roy S, Van Oyen H, Griffiths C, Michel J-P and Herrmann F R 2008 Death toll exceeded 70 000 in Europe during the summer of 2003 *C. R. Biol.* **331** 171–8

[21] Whitman S, Good G, Donoghue E R, Benbow N, Shou W and Mou S 1997 Mortality in Chicago attributed to the July 1995 heat wave *Am. J. Public Health* **87** 1515–8

[22] Ganguly A R, Steinhaeuser K, Erickson D J, Branstetter M, Parish E S, Singh N, Drake J B and Buja L 2009 Higher trends but larger uncertainty and geographic variability in 21st century temperature and heat waves *Proc. Natl Acad. Sci. USA* **106** 15555–9

[23] Meehl G A and Tebaldi C 2004 More intense, more frequent, and longer lasting heat waves in the 21st century *Science* **305** 994–7

[24] Meehl G A *et al* 2011 Climate system response to external forcings and climate change projections in CCSM4 *J. Clim.* **25** 3661–83

[25] Oleson K W *et al* 2010 Technical description of version 4.0 of the Community Land Model (CLM) *NCAR Technical Note* NCAR/TN-478+STR (Boulder, CO: National Center for Atmospheric Research)

[26] Thornton P E, Doney S C, Lindsay K, Moore J K, Mahowald N, Randerson J T, Fung I, Lamarque J F, Feddema J J and Lee Y H 2009 Carbon–nitrogen interactions regulate climate-carbon cycle feedbacks: results from an atmosphere–ocean general circulation model *Biogeosciences* **6** 2099–120

[27] Smith R D *et al* 2010 The Parallel Ocean Program (POP) reference manual: ocean component of the Community Climate System Model (CCSM) and Community Earth System Model (CESM) *Los Alamos National Laboratory Tech. Rep.* LAUR-10-01853 (Los Alamos, NM: Los Alamos National Laboratory)

[28] Bitz C M, Shell K M, Gent P R, Bailey D A, Danabasoglu G, Armour K C, Holland M M and Kiehl J T 2011 Climate sensitivity of the community climate system model, version 4 *J. Clim.* **25** 3053–70

[29] Smith R D, Dukowicz J K and Malone R C 1992 Parallel ocean general circulation modeling *Physica* D **60** 38–61

[30] Smith R D, Kortas S and Meltz B 1995 Curvilinear coordinates for global ocean models *Los Alamos National Laboratory Tech. Rep.* LA-UR-95-1146 (Los Alamos, NM: Los Alamos National Laboratory)

[31] Hunke E C and Lipscomb W H 2008 CICE: the Los Alamos Sea Ice Model, documentation and software, version 4.0 *Los Alamos National Laboratory Tech. Rep.* LA-CC-06-012 (Los Alamos, NM: Los Alamos National Laboratory)

[32] Holland M M, Bailey D A, Briegleb B P, Light B and Hunke E 2011 Improved sea ice shortwave radiation

[33] physics in CCSM4: the impact of melt ponds and aerosols on Arctic sea ice *J. Clim.* **25** 1413–30

[33] Skamarock W C and Klemp J B 2008 A time-split nonhydrostatic atmospheric model for weather research and forecasting applications *J. Comput. Phys.* **227** 3465–85

[34] Kain J S 2004 The Kain–Fritsch convective parameterization: an update *J. Appl. Meteorol.* **43** 170–81

[35] Lam Y F, Fu J S, Wu S and Mickley L J 2011 Impacts of future climate change and effects of biogenic emissions on surface ozone and particulate matter concentrations in the United States *Atmos. Chem. Phys.* **11** 4789–806

[36] Wong D C, Pleim J, Mathur R, Binkowski F, Otte T, Gilliam R, Pouliot G, Xiu A, Young J O and Kang D 2012 WRF-CMAQ two-way coupled system with aerosol feedback: software development and preliminary results *Geosci. Model Dev.* **5** 299–312

[37] Hong S-Y and Lim J-O 2006 The WRF single-moment 6-class microphysics scheme (WSM6) *J. Korean Meteorol. Soc.* **42** 129–51

[38] Janjić Z I 1990 The step-mountain coordinate: physical package *Mon. Weather Rev.* **118** 1429–43

[39] Mellor G L and Yamada T 1982 Development of a turbulence closure-model for geophysical fluid problems *Rev. Geophys.* **20** 851–75

[40] Chen F and Dudhia J 2001 Coupling an advanced land surface–hydrology model with the Penn State—NCAR MM5 modeling system. Part I: model implementation and sensitivity *Mon. Weather Rev.* **129** 569–85

[41] Lo J C-F, Yang Z-L and Pielke R A Sr 2008 Assessment of three dynamical climate downscaling methods using the Weather Research and Forecasting (WRF) model *J. Geophys. Res.* **113** D09112

[42] Iacono M J, Delamere J S, Mlawer E J, Shephard M W, Clough S A and Collins W D 2008 Radiative forcing by long-lived greenhouse gases: calculations with the AER radiative transfer models *J. Geophys. Res.* **113** D13103

[43] Morcrette J J, Barker H W, Cole J N S, Iacono M J and Pincus R 2008 Impact of a new radiation package, McRad, in the ECMWF integrated forecasting system *Mon. Weather Rev.* **136** 4773–98

[44] Deng A and Stauffer D R 2006 On improving 4-km mesoscale model simulations *J. Appl. Meteorol. Climatol.* **45** 361–81

[45] Meehl G A, Tebaldi C, Walton G, Easterling D and McDaniel L 2009 Relative increase of record high maximum temperatures compared to record low minimum temperatures in the U.S *Geophys. Res. Lett.* **36** L23701

[46] Riahi K, Grübler A and Nakicenovic N 2007 Scenarios of long-term socio-economic and environmental development under climate stabilization *Technol. Forecast. Soc. Change* **74** 887–935

[47] Soares P M, Cardoso R, Miranda P A, Medeiros J, Belo-Pereira M and Espirito-Santo F 2012 WRF high resolution dynamical downscaling of ERA-Interim for Portugal *Clim. Dyn.* **39** 2497–522

[48] Zhang Y, Duliere V, Mote P W and Salathe E P 2009 Evaluation of WRF and HadRM mesoscale climate simulations over the U.S. Pacific Northwest *J. Clim.* **22** 5511–26

[49] Nakicenovic N and Swart R 2000 *Special Report on Emissions Scenarios: A Special Report of Working Group III of the Intergovernmental Panel on Climate Change* (Cambridge: Cambridge University Press)

[50] Karl T R and Knight R W 1997 The 1995 Chicago heat wave: how likely is a recurrence? *Bull. Am. Meteorol. Soc.* **78** 1107–19

[51] Huth R, Kysely J and Pokorna L 2000 GCM simulation of heat waves, dry spells, and their relationships to circulation *Clim. Change* **46** 29–60

[52] Salinger M J and Griffiths G M 2001 Trends in New Zealand daily temperature and rainfall extremes *Int. J. Climatol.* **21** 1437–52

[53] Diffenbaugh N S, Bell J L and Sloan L C 2006 Simulated changes in extreme temperature and precipitation events at 6 ka *Palaeogeogr. Palaeoclimatol. Palaeoecol.* **236** 151–68